Slow-Binding Inhibition of *Escherichia coli* Cystathionine β-Lyase by L-Aminoethoxyvinylglycine: A Kinetic and X-ray Study[‡]

Tim Clausen,*,[§] Robert Huber,[§] Albrecht Messerschmidt,[§] Hans-Dieter Pohlenz,[∥] and Bernd Laber[⊥]

Max-Planck-Institut für Biochemie, Abteilung Strukturforschung, Am Klopferspitz 18a, D-82152 Martinsried, Germany, Institute of Cellular and Molecular Biology, Schering AG, D-13342 Berlin, Germany, and Hoechst Schering AgrEvo GmbH, Forschung Biochemie, D-65926 Frankfurt am Main, Germany

Received March 19, 1997; Revised Manuscript Received June 23, 1997[⊗]

ABSTRACT: The pyridoxal 5′-phosphate (PLP)-dependent cystathionine β-lyase (CBL) was previously found to be inhibited by the natural toxins rhizobitoxine and L-aminoethoxyvinylglycine (AVG). The present study characterizes the interaction of *Escherichia coli* CBL with AVG and methoxyvinylglycine (MVG) by a combination of kinetic methods and X-ray crystallography. Upon AVG treatment, time-dependent, slow-binding inhibition [Morrison, J. F. (1982) *Trends Biochem. Sci. 7*, 102−105] was observed due to the generation of a long-lived, slowly dissociating enzyme−inhibitor complex. Kinetic analysis revealed a one-step inhibition mechanism (CBL + AVG → CBLAVG, $K_i = 1.1 \pm 0.3$ μM) with an association rate constant (k_1) of 336 ± 40 M^{-1} s^{-1}. This value is several orders of magnitude lower than typical bimolecular rate constants of ES formation, suggesting that additional steps occur before formation of the first detectable CBLAVG complex. Loss of activity is paralleled by the conversion of the pyridoxaldimine 426 nm chromophore to a 341 nm-absorbing species. On the basis of the recently solved structure of native CBL [Clausen, T., et al. (1996) *J. Mol. Biol. 262*, 202−224], it was possible to elucidate the X-ray structure of the CBLAVG complex and to refine it to an *R*-factor of 16.4% at 2.2 Å resolution. The refined structure reveals the geometry of the bound inhibitor and its interactions with residues in the active site of CBL. Both the X-ray structure and the absorbance spectrum of the CBLAVG complex are compatible with a ketimine as the reaction product. Thus, the inhibitor seems to bind in a similar way to CBL as the substrate, but after α-proton abstraction, the reaction proceeds in a CBL nontypical manner, i.e. protonation of PLP-C4′, resulting in the "dead-end" ketimine PLP derivative. The CBLAVG structure furthermore suggests a binding mode for rhizobitoxine and explains the failure of MVG to inhibit CBL.

Cystathionine β-lyase (CBL,[1] EC 4.4.1.8, also commonly referred to as β-cystathionase) is a PLP-dependent enzyme that catalyzes the cleavage of L-cystathionine to L-homocysteine, pyruvate, and ammonia. An outline of this β-elimination reaction, showing the principal intermediates, is given in Scheme 1. Upon binding of the substrate cystathionine, the Michaelis complex **I** is rapidly converted *via* transaldimination to the external aldimine **II**, followed by α-proton abstraction to yield an α-carbanion equivalent stabilized as the ketimine quinonoid intermediate **III**. Subsequent elimination of L-homocysteine generates the PLP derivative of aminoacrylate **IV**. Protonation of the aminoacrylate and

Scheme 1

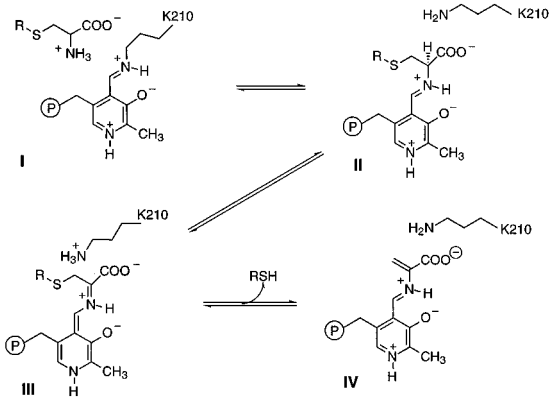

reverse transaldimination then form iminopropionate and regenerate the enzyme-bound PLP. Hydrolysis of iminopropionate to pyruvate and ammonia presumably occurs after product release. In addition to L-cystathionine, *Escherichia coli* CBL accommodates L-cystine, L-homolanthionine, *meso*-lanthionine, and L-djenkolic acid as substrates for β-elimination reactions (*1*).

Recently, the spatial structure of *E. coli* CBL has been determined by X-ray crystallography (*2*). The enzyme exists as an α_4 tetramer, constructed as a dimer of dimers, with 395 amino acids per subunit. Each monomer can be described in terms of three spatially and functionally different domains: (i) an N-terminal domain which contributes to

[‡] The coordinates of the CBLAVG complex have been deposited with the Brookhaven Protein Data Bank (filename 1CL2) and will be released with a delay of 1 year.

* Corresponding author. Phone: ++49-89-8578-2827. Fax: ++49-89-8578-3516.

[§] Max-Planck-Institut für Biochemie.

[∥] Schering AG.

[⊥] Forschung Biochemie.

[⊗] Abstract published in *Advance ACS Abstracts,* September 15, 1997.

[1] Abbreviations: F_o and F_c, observed and calculated structure factor amplitude, respectively; *I*, measured reflection intensity; *R*-factor, $\sum(|F_o|-|F_c|)/\sum|F_o|$; *B*-factor, thermal motion parameter $= 8\pi^2\hat{U}^2$, where $\hat{U}^2$ is the mean square amplitude of vibration; rms, root mean square; PLP, pyridoxal 5′-phosphate; CBL, cystathionine β-lyase; AVG, aminoethoxyvinylglycine; MVG, methoxyvinylglycine; CBLAVG, complex between CBL and AVG; ES, enzyme−substrate complex; EI, enzyme−inhibitor complex; Arg58*, * indicating a residue from the neighboring subunit of the catalytic active dimer.

S0006-2960(97)00630-2 CCC: $14.00

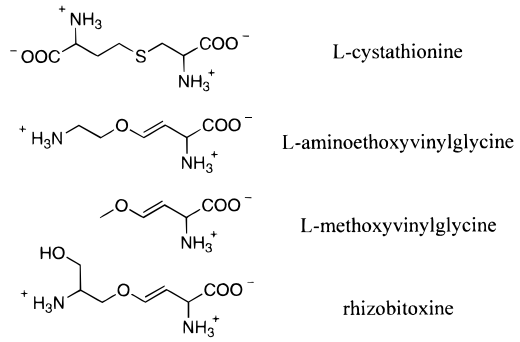

FIGURE 1: Structures of L-cystathionine, AVG, MVG, and rhizobitoxine.

tetramer formation and is part of the active site of the adjacent subunit, (ii) a large PLP-binding domain of α/β-structure with a seven-stranded β-sheet as its central part sandwiched between eight α-helices, and (iii) a C-terminal domain involved in substrate binding, which is connected by a long α-helix to the PLP-binding domain and consists of four helices packed on the solvent-accessible side of a four-stranded antiparallel β-sheet. The folds of the C-terminal and the PLP-binding domain and the location of the active site resemble very strongly the three-dimensional structures of various members of the α-family of PLP-dependent enzymes (*3*). Furthermore, most of the CBL active site residues are strictly conserved among the enzymes of the transsulfuration pathway, i.e. cystathionine β and γ-lyase and cystathionine β- and γ-synthase, which all belong to the so-called γ-family of PLP-dependent enzymes.

CBL is inhibited by the active site-directed irreversible inhibitor β,β,β-trifluoroalanine (*4*). The elucidation of the three-dimensional structure of CBL inactivated by trifluoroalanine (*2*) confirmed the reaction mechanism proposed for the inactivation of PLP-dependent enzymes by trihaloamino acids (*5*). In addition to trifluoroalanine, CBL is inhibited by L-aminoethoxyvinylglycine (AVG), an antimicrobial amino acid first isolated from *Streptomyces* sp. (*6*). Inhibition by AVG was characterized as time-dependent but reversible and was shown to be accompanied by a change in the absorption spectrum of the enzyme (*7*). Furthermore, CBL is the target of the antibacterial and phytotoxic amino acid rhizobitoxine (*8*−*11*), a close structural analog of AVG (Figure 1). Again, the inhibition is time-dependent, and reactivation of the inactivated enzyme by incubation with PLP suggests that inactivation is due to a modification of the PLP cofactor (*9*). Thus, inhibition of CBL by AVG and rhizobitoxine is likely to follow the same mechanism. However, the molecular basis for inhibition has not yet been elucidated.

Because CBL is involved in microbial and plant methionine biosynthesis, where it catalyzes the penultimate step, information on the mechanism of inhibition of CBL by any type of inhibitor, be it a classical, a slow/tight binding, or a suicide one, may facilitate the development of novel antimicrobial agents or herbicides. Therefore, we studied the interaction of *E. coli* CBL with AVG using kinetic and UV−visible spectral techniques. The results presented here provide direct evidence that AVG fulfills the criteria for a slow-binding inhibitor (*12*) of CBL. Furthermore, we elucidated the spatial structure of the CBLAVG complex by X-ray crystallography. An inhibition mechanism based on the kinetic, spectroscopic, and crystallographic data is proposed.

EXPERIMENTAL PROCEDURES

Materials. AVG was purchased from Fluka. Methoxyvinylglycine (MVG) was a gift of K. H. Neff (Schering AG, Berlin, Germany). The recombinant, overexpressed CBL from *E. coli* was purified as described previously (*13*) and was shown by SDS−PAGE to be >95% pure.

Enzyme Assay. CBL activity was assayed at 25 °C by detecting the amount of homocysteine produced over time (*14*). Assay mixtures contained 100 mM Tris/HCl (pH 8.5), 5 mM L-cystathionine, 1 mM 5,5′-dithiobis(2-nitrobenzoic acid), and enzyme in a final volume of 1 mL. The reaction was followed by recording the increase in absorbance at 412 nm with time.

In a typical inactivation experiment, CBL was preincubated at 25 °C in 100 μL of 100 mM Tris/HCl (pH 8.5) containing varying concentrations of inhibitor. At predetermined time intervals, 10 μL aliquots were transfered to 990 μL of the assay solution. Kinetic constants were determined from replots of the half-time for inactivation vs inhibitor concentration (*4*).

When CBL activity was assayed after addition of enzyme to assay mixtures containing an excess of substrate and inhibitor over enzyme, the resulting progress curves were fitted to equations adopted from Cha (*15, 16*), Morrison (*12*), and Morrison and Walsh (*17*) for the analysis of slow-binding inhibitors; i.e. $P = v_S t + (v_0 - v_S)\,[1 - \exp(-k_{obs}t)]/k_{obs}$, where P is the product concentration and v_0 and v_S are the initial and steady state velocities, respectively. The individual rate and inhibition constants were determined from replots of k_{obs} against the inhibitor concentration.

Protein Determination. Protein was determined by the method of Bradford (*18*) with bovine serum albumin as the standard. For spectral studies, the concentration of homogeneous CBL was calculated on the basis of the extinction coefficient at 280 nm of 51 105 M^{-1} cm^{-1} and a subunit weight of 43 312 Da.

Spectral Studies. Steady state absorbance spectra were recorded with a Kontron Uvikon model 930 spectrophotometer, using an optical path of 1.0 cm. Rapid reaction studies were carried out with a temperature-controlled stopped-flow apparatus constructed by Raichle (*19*) and equipped with a diode array (Spectrocopy Instruments GmbH). The optical path of this system was 2.0 cm. Data acquisition was performed with a Macintosh II cx computer using Posma software. All kinetic data were analyzed using fitting routines implemented in various software products [SPECFIT 2.0, Kaleidagraph 3.0, and the kinetic fitting program (program A) of D. P. Ballou (University of Michigan, Ann Arbor, MI)].

Binding of AVG to CBL is accompanied by a change in the absorption spectrum (see below). Spectral changes were followed at several inhibitor concentrations using the stopped-flow technique. Apparent pseudo-first-order rate constants, k_{obs}, were calculated by fitting the change in absorbance at 341 and 426 nm as a function of time to the single-exponential function $A = A_S + (A_0 - A_S)\exp(-k_{obs}\,t)$, where t is time, A_0 and A are the absorbances at time zero and at time t, respectively, and A_S is the final steady state absorbance. The individual rate and inhibition constants of the simple model

$$E + I \underset{k_2}{\overset{k_1}{\rightleftharpoons}} EI$$

were determined from replots of k_{obs} against the inhibitor concentration [I]: $k_{obs} = k_2 + k_1[I]$ and $K_i = k_2/k_1$.

UV Absorption Spectra of Crystals. Analysis of the spectral properties of crystals of the CBLAVG complex was performed with a single-beam Zeiss microspectrophotometer III linked to a HP9845B microcomputer using the LAMBDA-SCAN (Zeiss) software. The light from the xenon lamp (250−700 nm) was monochromated by a grating monochromator. The objective was an Ultrafluar 32/0.40 with a glycerol drop placed between the sample holder and the objective lens. The crystals were placed between a quartz plate and a quartz cover slip that were separated by cover slips that were 0.12 mm thick. The dimension of a typical crystal, suitable for spectral analysis, was 0.06 × 0.03 × 0.03 mm^3.

Crystallographic Methods. Prior to crystallization, *E. coli* CBL (10 mg/ml) was preincubated with 20 mM AVG until the 426 nm absorption maximum of the uninhibited enzyme was completely bleached. Crystals of the CBLAVG complex were then grown overnight by the hanging drop vapor diffusion method, using the conditions described for crystallization of the uninhibited enzyme (*13*). Diffraction data were collected using an imaging plate scanner (MAR research) and graphite monochromatized CuKα radiation from a RU200 rotating anode (Rigaku, Tokyo, Japan) operated at 5.4 kW. The apparent focal spot size was set to 0.3 mm × 0.3 mm. Data sets were obtained by rotating the crystal about *c** parallel to the spindle axis for 90° with a rotation range of 1° per image. Reflection data were processed using the MOSFLM package (*20*), and subsequently, the intensities were scaled, reduced, and truncated to structure factors using programs from the CCP4 program suite (*21*). The CBLAVG data sets were collected from one crystal each and showed the same space group and cell parameters as the uncomplexed CBL crystals ($C222_1$ with a = 61.1 Å, b = 154.7 Å, and c = 152.3 Å), allowing the native phases to be used to solve the structure. Refinement was carried out with the program XPLOR (*22*). Manual rebuilding between refinement cycles and model examination was done with the program O (*23*) running on an ESV-30 graphics station (Evans & Sutherland, Salt Lake City, UT). To calculate an initial $F_o - F_c$ electron density map, the coordinates of the uncomplexed CBL structure were used, from which the bicarbonate ion, located in the active site of the active enzyme, and all water molecules had been excluded. Clear, continuous density was observed which extends from the cofactor into the active site, indicating a covalent inhibitor−PLP adduct. A model of the inhibition complex was built into the density and refined to convergence. The final *R*-factor was 16.4% for all data between 8.0 and 2.2 Å with good geometry for the model (Table 1).

Table 1: Parameters of the Refined Model

no. of active protein atoms	5959
no of active cofactor atoms	54
no. of active solvent molecules	430
R-factor of final model[a] (%)	16.4
no. of unique reflections	35 500
standard deviation from ideal values	
bond lengths (Å)	0.01
bond angles (deg)	1.89
temperature factors (Å^2)	
all atoms	16.9
main chain atoms	15.9
side chain atoms	18.1
PLP-AVG atoms	16.3
solvent molecules	28.6

[a] The *R*-factors were calculated in the resolution range of 8.0− 2.20 Å.

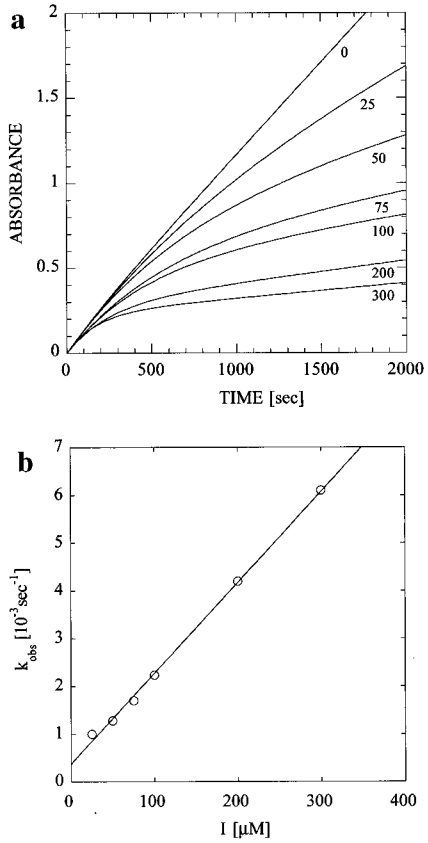

FIGURE 2: Inhibition of CBL activity after addition of CBL (30 μg) to an enzyme assay mixture containing 5 mM L-cystathionine and different inhibitor concentrations. (a) Reaction progress curves at inhibitor concentrations of 0, 25, 50, 75, 100, 150, 200, and 300 μM. (b) Replot of k_{obs} vs L-AVG concentration. k_{obs} is derived from the progress curves as described in Experimental Procedures.

RESULTS

Inhibition by AVG. When CBL activity was continuously assayed after addition of enzyme to assay mixtures containing both AVG and L-cystathionine, the resulting progress curves displayed a time-dependent decrease in reaction rate and finally attained a steady state velocity which varies as a function of inhibitor concentration (Figure 2a), suggesting the slow establishment of an equilibrium between enzyme, inhibitor, and the enzyme−inhibitor complex. Thus, AVG acts as a slow-binding inhibitor (*12*). Further evidence for slow-binding inhibition was obtained by adding aliquots of preincubation mixtures of CBL and AVG to substrate-containing assay mixtures. The resulting progress curves displayed a time-dependent increase in reaction rate and reached a steady state velocity identical to the velocity obtained without preincubation. Enzyme added to the inhibition cocktail at times when maximal inhibition has been achieved was also inhibited, excluding the possibility that the observed steady state levels are due to the disappearance of AVG during incubation with CBL (e.g. decomposition in solution or enzyme-catalyzed modification). The rate of enzyme inactivation was highly dependent on the pH of the preincubation mixture and showed the same pH dependence as substrate turnover (for 20 μM AVG, the half-time of inhibition $t_{1/2}$ was 180 min at pH 7.0 and 0.4 min at pH 9.0).

Table 2: Different Mechanisms of Slow-Binding Inhibition and Their Relationship to the Apparent First-Order Constant k_{obs}

mechanism	model	k_{obs}
A	$E \underset{k_2}{\overset{k_1[I]\text{(slow)}}{\rightleftharpoons}} EI$	$k_2\left[1+\frac{[I]}{K_i(1+[S]/K_m)}\right]^a$
B	$E \underset{k_2}{\overset{k_1[I]}{\rightleftharpoons}} EI \underset{k_4}{\overset{k_3\text{(slow)}}{\rightleftharpoons}} EI^*$	$k_4\left[\frac{1+\frac{[I]}{K_i^*(1+[S]/K_m)}}{1+\frac{[I]}{K_i(1+[S]/K_m)}}\right]^b$
C	$E \underset{k_2}{\overset{k_1\text{(slow)}}{\rightleftharpoons}} E^* \underset{k_4}{\overset{k_3}{\rightleftharpoons}} E^*I$	$\frac{k_1}{1+[S]K_M}+\frac{k_2K_i}{[I]+K_i}^c$

[a] $K_i = k_2/k_1$. [b] $K_i^* = k_4K_i/(k_3 + k_4)$. [c] $K_i = k_4/k_3$.

As indicated in Table 2, there are three simple mechanisms which can account for a slow onset of inhibition (*12*, *17*). Mechanism A corresponds to an initial slow-binding process. In mechanism B, an EI complex is formed rapidly and then undergoes slow isomerization (conformational change) to a slowly dissociating EI* complex. In a third variant, mechanism C, the enzyme itself must slowly isomerize before it can bind inhibitor.

The kinetic analysis of the reaction progress curves recorded at pH 8.5 for AVG concentrations of up to 300 μM revealed that the initial reaction velocities (v_0) were independent of inhibitior concentration (Figure 2a). Furthermore, a replot of k_{obs} against the inhibitor concentrations (Figure 2b) gave a straight line with no indication of saturation kinetics. Both features indicate the direct formation of a slowly dissociating EI complex without the initial formation of a rapidly reversible enzyme−inhibitor complex. Further evidence for mechanism A was obtained by plotting $1/(k_{obs} - k_2)$ vs $1/[I]$. The resulting straight line passes through the origin which is consistent with mechanism A. A dissociation constant K_i of 1.1 μM and a rate constant k_2 of 3.7×10^{-4} s^{-1} were obtained from a fit of k_{obs} to the equation $k_{obs} = k_2 + k_2[I]/[K_i(1 + [S]/K_m)]$. A value for k_1 of 336 M^{-1} s^{-1} was calculated using the expression $K_i = k_2/k_1$.

Spectral Changes Induced by AVG. Steady state absorbance spectra recorded at pH 8.5 immediately after mixing of CBL with AVG showed the complete loss of the pyridoxaldimine absorbance at 426 nm and the appearance of a new chromophore at 341 nm (ϵ = 27 500 M^{-1} cm^{-1}). When the experiment was performed at pH values below 8.0, qualitatively identical spectral changes were observed, but they occurred more slowly. The decrease in intensity of the 426 nm chromophore was paralleled by an increase in absorbance at 341 nm, and there was a single isosbestic point at 386 nm.

Rapid scanning stopped-flow spectroscopic studies (Figure 3a) of the reaction of CBL with AVG in the concentration range of 0.05−1.5 mM showed that both the decrease of the 426 nm chromophore and the increase of the 341 nm chromophore can be fitted to a simple exponential model. The k_{obs} values calculated for each of these spectral changes were identical within experimental error (Figure 3b). A replot of k_{obs} vs inhibitor concentration gave a straight line with a slope corresponding to k_1 of 153 M^{-1} s^{-1} and a vertical intercept giving a k_2 of 4.5×10^{-3} s^{-1}. Since the *y*-intercept is close to the origin, the potential error of the k_2 value is high.

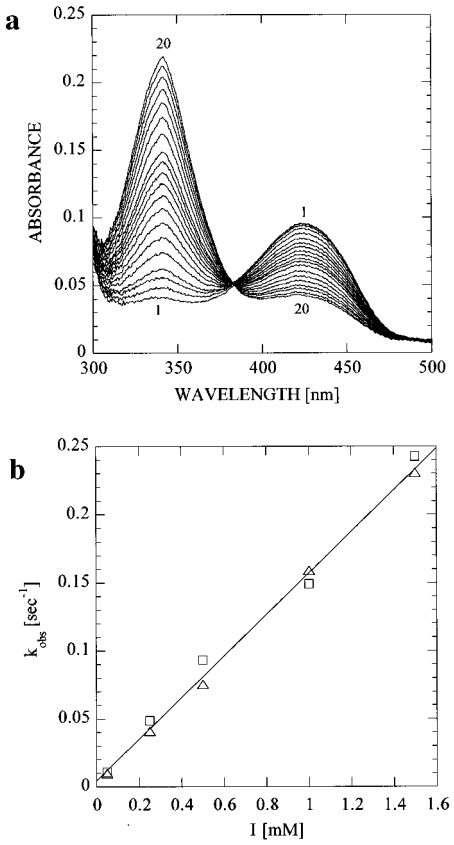

FIGURE 3: Stopped-flow kinetic measurements of slow-binding inhibition by L-AVG. (a) Absorbance spectra of the reaction of 10 μM CBL with 1.5 mM L-AVG in 100 mM Tris/HCl buffer (pH 8.5). The spectra were collected at 20 °C with a diode array in 50 ms intervals after mixing. Lane 1 corresponds to the first spectrum collected after 100 ms and lane 20 to the last one collected after 1 s. (b) Replot of k_{obs} vs AVG concentration. k_{obs} was determined by following spectral changes at 341 nm (□) and 426 nm (△).

Reversibility of Inhibition by AVG. The reversibility of inhibition of CBL by AVG was tested by gel filtration of the inhibited enzyme which resulted in only a slight (about 10%) recovery of catalytic activity. However, after removal of free AVG by gel filtration, CBL in the now AVG-free buffer slowly regained enzymatic activity (up to 100%). The recovery of enzymatic activity was paralleled by a decrease of the 341 nm absorbance, characterizing the inhibited enzyme, and by the reappearance of the 426 nm chromophore observed in fully active CBL (Figure 4). A good isosbestic point was observed at 386 nm. The half-time of enzyme−inhibitor complex dissociation, determined by following the spectral changes and the regain of enzyme activity, was about 5 h.

Reaction with MVG. MVG is a bacterial toxin isolated from fermentation broths of *Pseudomonas aeruginosa* (*24*). It irreversibly inactivates L-aspartate aminotransferase (*25*) and is both a substrate and inactivator of *E. coli* tryptophan synthase (*26*). The interaction of CBL with MVG, which can be regarded as an analog of AVG missing the terminal aminomethyl part of the molecule, was investigated to study the contribution of the terminal amino group to the inhibitory potency of AVG. MVG, even after prolonged preincubation in the absence of substrate, did not significantly inhibit CBL. Steady state absorbance spectra obtained during the enzymatic processing of MVG were characterized by a decrease in absorbance at 426 nm followed by the slow accumulation of a new chromophore at 486 nm (ϵ = 2500 M^{-1} cm^{-1}; Figure 5) and an absorbance increase in the region of 300−

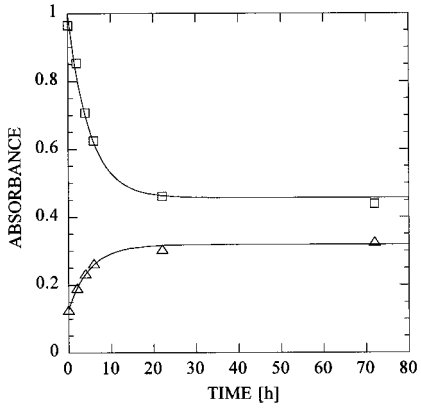

FIGURE 4: Recovery of CBL activity in L-AVG-free solution (100 mM Tris/HCl at pH 8.5 and 4 °C). The half-time of activity regain was determined by following the reappearance of the 426 nm (△) and the loss of the 341 nm maximum (□). A single-exponential fit yielded in both cases a $t_{1/2}$ of 5 h.

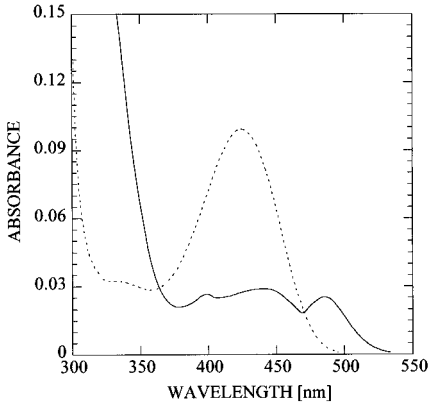

FIGURE 5: Absorbance spectra of 15 μM CBL in 100 mM Tris/HCl at pH 8.5. Spectra were collected at 20 °C (dotted line) prior to and (solid line) 300 min after addition of 2 mM MVG.

350 nm and below 280 nm. Since the short-wavelength absorbance changes are characteristic for the absorbance of α-keto acids, the assay solutions were subjected to α-keto acid analysis by reversed-phase HPLC after precolumn derivatization with 1,2-phenylenediamine (*27*). In the eluate of the reversed-phase HPLC column, a peak representing the major product keto acid (74%) was observed, which did not coelute with any of the commercially available α-keto acid standards (containing up to six carbon atoms), together with pyruvate (23%) and a small amount of α-ketobutyrate (3%). The major product peak could not unequivocally be identified as 2-oxo-4-methoxybutanoate due to the lack of an appropriate standard. However, failure of MVG to inhibit the enzyme implies that the terminal amino group of AVG is essential for inhibition of CBL.

Crystal Structure of CBL Inhibited by AVG. A prerequisite for the deduction of an inhibition mechanism from crystallographic data is the demonstration that the crystallographic enzyme−inhibitor complex is identical with the enzyme−inhibitor complex formed in solution. When we measured a spectrum of a CBLAVG crystal, we obtained the features characteristic for CBL inhibited by AVG in solution: an absorption maximum at 341 nm and the complete loss of the 426 nm spectral band. This was taken as sufficient evidence for the formation of identical enzyme−inhibitor complexes in the crystal and in solution.

The structure of the CBLAVG complex was solved at 2.2 Å resolution. The final model includes 430 water molecules and exhibits the same stereochemistry as the native structure [PROCHECK (*28*)]. There are no significant changes in the overall CBL structure. The average α-carbon rms deviation between the two models is 0.159 Å. The configuration of the bound inhibitor was clear and unambiguous, both in the initial $F_o - F_c$ and in the final $2F_o - F_c$ electron density maps. Stereoviews of the refined model of the PLP−inhibitor complex with its respective electron densities superimposed (Figure 6) give an indication of the quality of the X-ray structure.

The electron density clearly indicates covalent binding of the inhibitor to C4′ of the cofactor (for nomenclature, see Figure 7a). Furthermore, the electron density in this part of the adduct suggests sp^3 and sp^2 hybridization for C4′ and CAI, respectively, which is consistent with a ketimine reaction product. Figure 7a shows a schematic view of this ketimine built into the active site of CBL, indicating specific interatomic distances, hydrogen bonds, and van der Waals interactions. The spatial arrangement of selected active site residues is given in Figure 7b.

The inhibitor is bound strongly by several ionic, hydrogen bonding, and van der Waals interactions. The α-carboxylate group of the complexed AVG is located in the same position as the bicarbonate ion in the native and the α-carboxylate group of trifluoroalanine in the trifluoroalanine-inactivated CBL structure. The α-carboxylate group forms a double-hydrogen-bonded ion pair, optimized by coplanar arrangement, with the positively charged Arg372−guanidinium group. Additional hydrogen bonds are formed with the backbone nitrogen NH of Ser339, the NE1 of Trp340, and a well-defined active site water molecule (HOH2). The *B*-factors of the α-carboxylate group are ∼15 Å^2, as is the average *B*-factor of the surrounding atoms, thus indicating an inhibitor occupancy of 1.0. In contrast, the inhibitor occupancy for trifluoroalanine-inactivated CBL was proposed to be 0.5 (*2*). The atomic *B*-factors of AVG increase from 15 to 30 Å^2 in the direction toward the terminal amino group, suggesting an increase in flexibility. The terminal amino group of AVG is held in place mainly by interactions with the hydroxyl group of Tyr111. Interestingly, this hydroxyl group is also close to CGI, offering a possibility for proton transfer. Additionally, the terminal amino group forms two strong hydrogen bonds with two well-defined water molecules which have no positional equivalents in the native structure. One of these molecules, HOH4, is mediating an indirect interaction between the terminal amino group of AVG and the hydroxyl group of Tyr238*. Furthermore, the phenolic rings of Tyr56* and Tyr338 are in van der Waals contact with CFI, CEI, and OET of the inhibitor, enclosing it within a pocket.

The active site structure of CBL has undergone some changes as a consequence of inhibitor binding (Figure 7c). While the phosphate group of the cofactor remains fixed, the pyridine ring reorients by rotation around bonds between the phosphorus atom and the pyridine ring, mainly by rotation around C5−C5′ of 15° in the manner suggested by Ivanov and Karpeisky (*29*). The OP4−C5′−C5−C6 torsion angle assumes a value of −96° as compared to −111° in the uncomplexed CBL, resulting in a cofactor tilt of 30° with respect to the pyridine ring plane in the native structure. The C3−C4−C4A−N4A torsion angle of −39° implies a perturbation of the coplanar arrangement of N4A, CAI, and the pyridine ring system, again suggesting a ketimine rather than an aldimine structure for the AVG−PLP complex. The

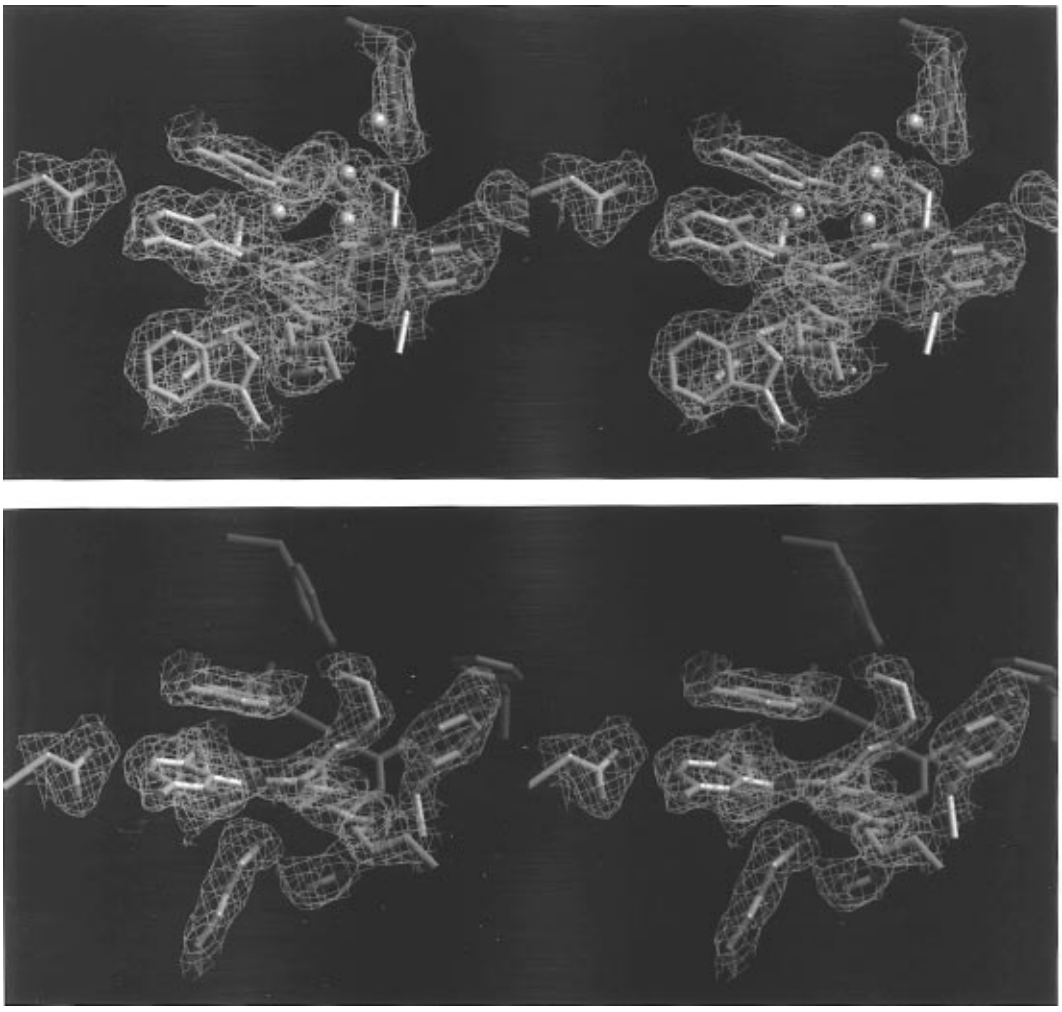

FIGURE 6: Stereoplot of the electron density in the active site of the L-AVG-inhibited CBL with the refined model of the EI adduct superimposed. The $2F_o - F_c$ difference Fourier map of the reaction product is contoured at 1.0σ and calculated at 2.2 Å resolution. To give a better impression of the quality of the structure, the electron density of the CBLAVG complex is shown in two orientations (a, top, and b, bottom).

phenolic ring of Tyr111 follows the movement of the cofactor and rearranges itself parallel to the pyridine ring. Due to the interaction of Tyr111 with the terminal amino group of AVG, the stacking interaction between the phenolic ring of Tyr111 and the pyridine ring of the cofactor is reduced. The backbone and side chain atoms of residues 338 to 340, which are directly involved in inhibitor binding, have shifted their position slightly toward the inhibitor. Especially the phenolic ring of Tyr338 reorients itself by rotating around Cβ−Cγ, thereby optimizing van der Waals contacts with the inhibitor.

Clearly, there is no electron density indicative of a covalent bond formed beween the inhibitor and CBL (Figure 6b). The side chains of Lys210 and Tyr111, which are the only suitable candidates for covalent bond formation, are both well-defined and are not closer than hydrogen bonding distance to the inhibitor. This rules out common inhibition mechanisms proposed for the inhibition of PLP-dependent enzymes by β,γ-unsaturated amino acid analogs (*30*) which involve covalent binding of the inhibitor to an active site nucleophile of the enzyme as has been experimentally established for the aspartate aminotansferase (*31*).

DISCUSSION

In the following, we will propose a reaction mechanism for slow-binding inhibition of CBL by AVG based on inactivation studies, analysis of spectral changes, and the crystal structure of the complex. The three-dimensional structure furthermore can explain the failure of MVG to inhibit CBL, suggests a binding mode for rhizobitoxine, and leads to deeper insight into the reaction mechanism of the γ-family of PLP-dependent enzymes.

Mechanism of Inhibition of CBL by AVG. Several β,γ-unsaturated amino acids have been described as irreversible inhibitors of PLP-dependent enzymes (*4*). The data presented here clearly demonstrate that inhibition of CBL by AVG is not an irreversible process, since enzymatic activity is regained after dilution of the inactivated enzyme into inhibitor-free assay mixtures and after removal of free inhibitor by gel filtration. Instead, inhibition of CBL by AVG obeys a slow-binding mechanism.

To date, nearly all reported examples of slow-binding inhibition exhibit biphasic inhibition kinetics due to the rapid formation of an initial enzyme−inhibitor (EI) complex followed by slow isomerization to a tighter EI* complex [mechanism B of Morrison (*12*) and Morrison and Walsh (*17*)]. However, our kinetic data indicate that inhibition of CBL by AVG proceeds *via* the single-step mechanism A, in which slow binding of the inhibitor results in the direct formation of a stable, slowly dissociating EI* complex ($K_i = 1.1\ \mu$M). On the other hand, the spectral changes observed upon inhibitor binding suggest that the inhibition mechanism

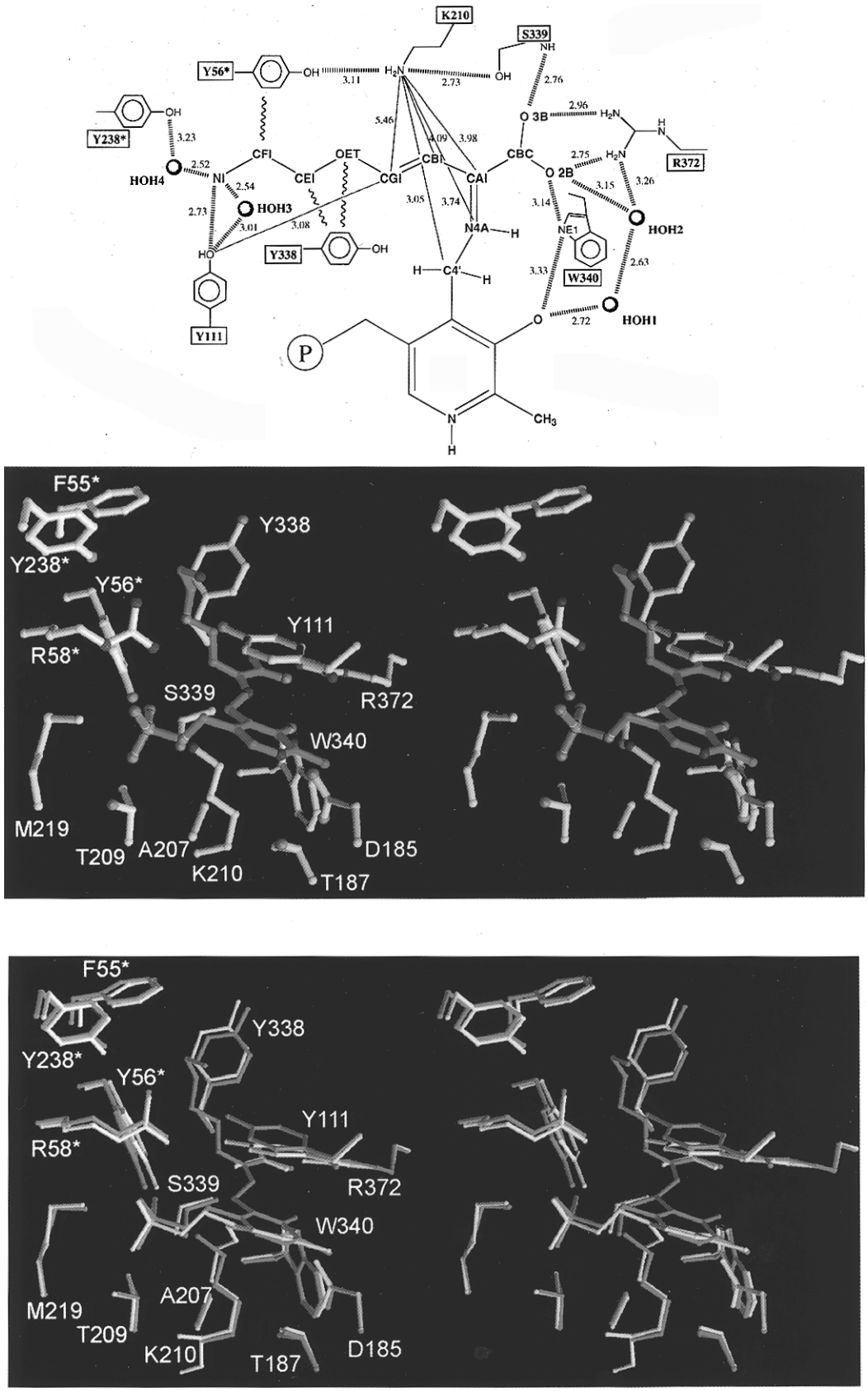

FIGURE 7: Plots showing the active site of the CBLAVG complex and its comparison with the native structure. The numbering of the atoms is standard with the exception of the inhibitor-derived atoms. The nomenclature of these atoms is given in panel a (top) which presents a schematic view of the active site, illustrating hydrogen bonds (- - -) and van der Waals interactions (∼∼) with interatomic distances given (- - -). Residues of the second subunit are labeled with an asterisk (*), and only four mechanistically interesting water molecules are shown (see Figure 6a). (b, middle) Stereoplot of the CBLAVG active site. (c, bottom) Stereoplot of the superposition of the active sites of CBLAVG (green) and native, unliganded CBL (gray).

should involve at least transaldimination and α-proton abstraction, thus favoring mechanism B. Furthermore, the bimolecular rate constant for inactivation k_1 of 336 M^{-1} s^{-1} is several orders of magnitude smaller than typical bimolecular rate constants for ES formation [10^5 −10^7 M^{-1} s^{-1} (*32*); 8.5 × 10^4 M^{-1} s^{-1} for turnover of L-cystathionine by

CBL] which also implies that more than one step is required for formation of the EI* complex (*17*). This mechanistic discrepancy can most likely be rationalized by assuming a special case of mechanism B, in which K_i is much greater than the overall dissociation constant K_i*; i.e. the inhibitor binds weakly to the free enzyme to form the EI complex (K_i in the high millimolar range), followed by a slow conversion to a tightened EI* complex (K_i* in the micromolar range). When the inhibitor concentration is now varied in the region of K_i*, i.e. [I] $\ll K_i$, the rate equation for k_{obs} in mechanism B (Table 2) is simplified to $k_{obs} = k_4[1 + [I]/[K_i*(1 + [S]/K_m)]]$. Under these conditions, k_{obs} appears to depend linearly on [I] and mechanism B is kinetically indistinguishable from mechanism A.

Treatment of CBL with AVG resulted in the rapid and complete loss of the pyridoxaldimine absorbance of the catalytically active enzyme at 426 nm and the concomitant formation of a 341 nm chromophore (Figure 3a). Using rapid scanning stopped-flow spectroscopy, these absorbance changes could be time-resolved and a good isosbestic point was observed at 386 nm, indicating that the two chromophores interconvert directly and that there are no kinetically important, well-populated intermediates. These findings are consistent with the interpretation of the kinetic data. Furthermore, upon recovery of enzymic activity of fully inhibited CBL, both reappearance of the 426 nm chromophore at the expense of the 341 nm chromophore and an isosbestic point at 386 nm were observed. Thus, recovery of enzymatic activity apparently is due to direct reversal of the inhibition reaction and not due to turnover of enzyme-bound inhibitor. Since the recovery of catalytic activity is independent of external PLP, dissociation of a modified cofactor from the active site followed by binding of fresh PLP can be excluded as a cause of reactivation.

Examples of slow-binding inhibition of PLP-dependent enzymes are scarce, being limited to 1-aminocyclopropanecarboxylate deaminase (*33*) and alanine racemase (*34*, *35*). For the latter enzyme, only the partial structural detail of the enzyme inhibitor complex, i.e. the presence of a protonated imine linkage to the cofactor, has been elucidated yet (*36*). The mechanistic reasons for slow-binding inhibition of PLP-dependent enzymes and the structure of the enzyme−inhibitor complexes are unclear so far. Our structural, kinetic, and spectroscopic data in combination with the reactivation of CBL in the absence of free PLP rule out the two most widely accepted mechanisms for inhibition of PLP-dependent enzymes by alkene-containing amino acid analogs: (a) activation of the inhibitor to a PLP-bound reactive intermediate which acts as a Michael acceptor for an active site nucleophile to give a covalently modified enzyme and (b) generation of an eneamine−PLP species which liberates the free eneamino acid that subsequently attacks the internal aldimine to yield inactive enzyme due to covalent modification of PLP (*4*).

The electron density of the enzyme−inhibitor adduct was helpful in the interpretation of the AVG-induced spectral changes. As illustrated in Scheme 2, the 341 nm chromophore of the fully inhibited enzyme is consistent with either a geminal diamine **VI**, a deprotonated imine **VIII**, a ketimine **IX**, or a pyridoxamine phosphate (PMP) **X**. The deprotonated imine **VIII** is unlikely to be the 341 nm chromophore, because formation of the chromophore occurred even at pH 6.0, but the deprotonated imine should be present only at high pH. PMP **X** also is an unlikely candidate

Scheme 2

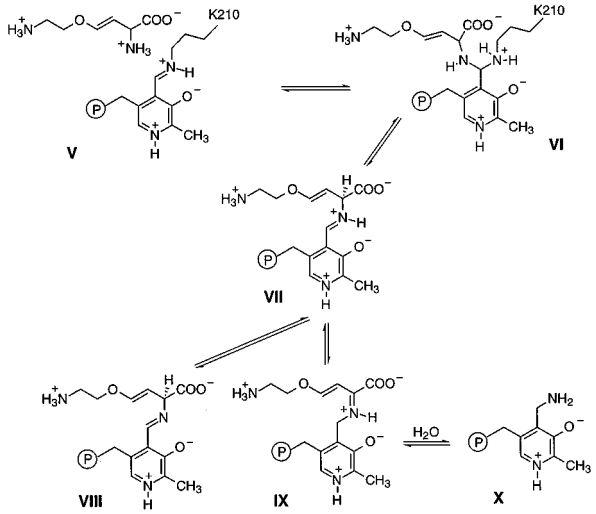

for the 341 nm chromophore, since both the absorbance maximum and extinction coefficient of PMP ($\epsilon_{327} = 9400$ M^{-1} cm^{-1}; *37*) differ significantly from the corresponding values of the 341 nm chromophore ($\epsilon_{341} = 27\,500$ M^{-1} cm^{-1}). Consistently, PMP could not be detected by reversed-phase HPLC after denaturation of fully inactivated CBL (data not shown). To further exclude the possibility of formation of a PMP species during AVG inhibition, we investigated the effect of a high concentration of an α-keto acid in the reaction mixtures. Reactivation was not affected by pyruvate, and also, the spectral changes observed upon inhibitor binding did not change qualitatively. Therefore, the 341 nm absorbance most likely arises from the ketimine intermediate **IX**, in accordance with the X-ray structure, which clearly excludes the geminal diamine **VI** as the AVG−PLP adduct and favors sp^3 and sp^2 conformations at C4′ and CAI, respectively.

On the basis of the structural and spectral features, we propose the following mechanism of inhibition of CBL by AVG. By analogy to the substrate cystathionine, the inhibitor enters the active site cleft from a position above Arg58* and Tyr111 (in the orientation of Figure 7b) to form the Michaelis complex **V**. Arg372, Tyr111, the ionized PLP hydroxyl group, and Tyr238* direct the inhibitor into the proper orientation for transaldimination. Since substrate turnover and enzyme inhibition show similar pH dependencies, it can be assumed that the same acid−base groups at the CBL active site are involved in both transaldimination reactions. Thus, Tyr111 is proposed to abstract a proton from the α-amino group of the incoming inhibitor, thereby initiating nucleophilic attack at C4′ and formation of the geminal diamine **VI**. After displacement from the geminal diamine, Lys210 is optimally positioned and oriented to act as a general base for abstracting Hα of the external aldimine **VII**. Although the electronic arrangement of the cofactor is now optimized for the stabilization of the resulting carbanion as a quinonoidal intermediate (readily detectable as the 497 nm chromophore during substrate turnover), it was not possible to detect any long-wavelength chromophores during the inactivation of CBL by AVG or during the reactivation process. Probably, quinonoid formation is made unfavorable by reduced ring-stacking interactions between the pyridine ring of the cofactor and the phenolic ring of Tyr111 upon inhibitor binding. Ring-stacking interactions have been shown to be essential in the reaction

mechanism of aspartate aminotransferase (*38*). Instead, it can be inferred from interatomic distances in the enzyme−inhibitor complex (Figure 7a) that the ϵ-amino group of Lys210 transfers the Hα proton directly from CAI to C4′. During this process, the positively charged ϵ-amino group of Lys210 is attracted by the negatively charged phosphate group of the cofactor, thereby approaching C4′ to within hydrogen bonding distance. After protonation of C4′ (i.e. formation of the ketimine **IX**), the uncharged ϵ-amino group of Lys210 is held in place by interacting with Ser339-OH and Tyr56*-OH.

Overall, our study reveals that AVG binds to CBL in a similar manner as a normal substrate, but after α-proton abstraction, the reaction proceeds in an unusual manner for CBL.

The relative stability of the resulting PLP−ketimine might arise from the inability of CBL to catalyze the transamination of AVG. Hydrolysis of the ketimine **IX** to PMP **X** and the corresponding α-keto acid is unlikely to occur since all water molecules that could be involved in hydrolysis (HOH1, HOH2, and HOH3) exhibit low *B*-factors (<15 Å^2), indicating their tight binding in the active site of the inhibited enzyme. Furthermore, Tyr225 of aspartate aminotransferase, which is believed to bind an incoming water molecule and initiate ketimine hydrolysis (*39*), has no equivalent counterpart in CBL. Thus, it seems that CBL suffers from its relationship to other cystathionine-utilizing enzymes, in which similar β,γ-unsaturated ketimines have been proposed to be important catalytic intermediates (*40*).

The overall dissociation constant K_i* of 1.1 μM suggests that AVG binds about 300-fold more tightly to CBL than does L-cystathionine ($K_m = 0.33$ mM). However, since K_i* does not represent a true dissociation constant, but rather includes an EI to EI* isomerization step, inhibition of CBL by AVG is mainly caused by the slow-dissociating properties of the reaction end product. As argued previously, the true K_i value of AVG should be much higher than 1.1 μM. Indeed, AVG is lacking the terminal carboxylate group which is thought to interact with an arginine of the adjacent subunit and thereby establish productive binding, as has been shown for aspartate aminotransferase (*41*−*43*). Congruently, the *B*-factors in this part of the inhibitor are 2 times higher than the atomic *B*-factors near Cα, indicating an increased flexibility of the distal part of the molecule and an unfavorable binding mode.

The spectral changes induced by AVG closely parallel the inactivation process. While differences in the k_1 rate are rather small, the k_2 rates are quite different. This difference might be due to experimental problems (e.g. the extreme pH dependence of CBL-catalyzed reactions) or due to slight, kinetically and spectrally silent changes in the active site environment which lead to further tightening of the EI* complex. However, the spectral changes should correspond directly to the slow approach to the steady state velocity observed in the inhibition assays.

From reactivation experiments, the half-life of the enzyme−inhibitor complex was determined to be about 300 min, which seems long enough to achieve significant *in vivo* inhibition of CBL, thus providing evidence for inhibition of CBL as a reason for the antibacterial activity of AVG.

Mechanism of the Reaction with MVG. MVG has previously been shown to be either a substrate or an irreversible inhibitor for various PLP-dependent enzymes (*25*, *26*, *30*, *44*). MVG does not inactivate CBL but is utilized as a substrate. Deamination of MVG is assumed to proceed by the mechanism proposed by Miles (*26*) and Johnston (*44*), which involves (a) α-proton abstraction from the pyridoxaldimine adduct **XI**, (b) azaallylic isomerization, which converts the pyridoxalketimine quinonoid **XII** to the eneamino adduct **XIII**, (c) reverse transaldimination liberating the product eneamino acid, and finally (d) hydrolysis of the tautomeric imino acid to yield 2-oxo-4-methoxybutanoate **XIV** as the product (Scheme 3). During deamination of MVG, a 486 nm chromophore is observed (Figure 5). The absorption spectrum of this chromophore, its low extinction coefficient, and the 11 nm shift of this maximum to the short-wavelength side of the spectrum relative to the 497 nm chromophore observed during L-cystathionine turnover imply that it is caused by the eneamino adduct **XIII** and does not represent the quinonoid intermediate **XII**. Due to its extended system of conjugated double bonds, quinonoid **XII** is predicted to absorb above 500 nm. This is supported by the observation of chromophores assigned to **XII** at 510 nm during reaction of tryptophan synthase with MVG (*26*) and at 550 nm in nonenzymatic model reactions (*45*). Thus, deamination of MVG apparently does not require the stabilization of a kinetically competent quinonoidal intermediate to a significant extent. Accumulation of the 486 nm chromophore is evidence that reverse transaldimination of **XIII** or hydrolysis of the product imino acid is the rate-limiting step in the deamination reaction.

Scheme 3

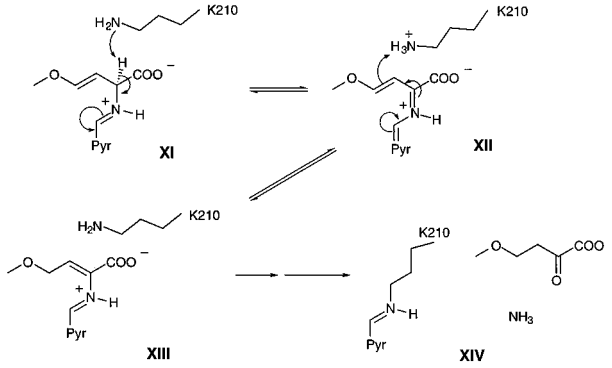

It is the terminal amino group that makes the difference between the substrate MVG and the inhibitor AVG. Due to the presence of this group, the aliphatic side chain of AVG becomes fixed in a position, in which it is impossible for the ϵ-amino group of Lys210 to interact with either Cβ or Cγ. The absence of the terminal amino group makes rotation around the Cα−Cβ bond possible and enables MVG to adopt a conformation which allows protonation of Cβ by Lys210 in accordance with Scheme 3.

General Implications. Rhizobitoxine is a close structural analog of AVG with an additional CH_2OH group at the distal part of the molecule (Figure 1). Kinetic parameters and X-ray data of the rhizobitoxine−CBL complex have not been determined by us yet, due to difficulties in the preparation and/or isolation of the toxin. However, the interaction of rhizobitoxine with CBL in many features resembles the interaction of CBL with AVG (*9*) and thus is likely to follow the same reaction mechanism including transaldimination, α-proton abstraction, and ketimine formation. Therefore, a model of the CBL−rhizobitoxine adduct was built using the crystal structure of the CBLAVG complex as a starting point. Standard values for angle and bond lengths (*46*) were used to optimize the model with XPLOR (*22*). During electro-

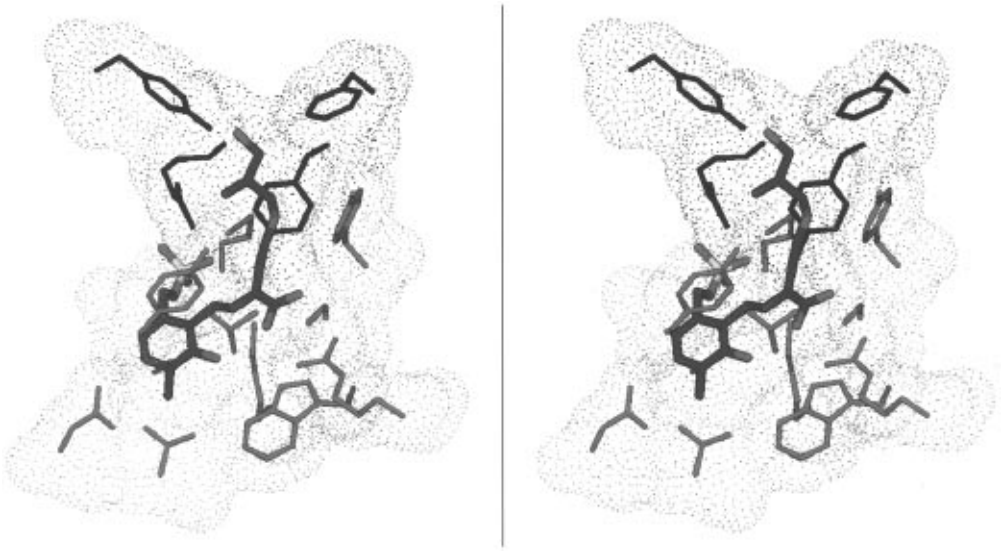

FIGURE 8: Hypothetical model of the EI complex between *E. coli* CBL and rhizobitoxine. The inhibitor bound to the cofactor is colored in atom color mode, and residues from the apoprotein are colored magenta and blue (adjacent subunit of the active dimer). The proteinous groups are overlaid with the corresponding Connolly dot surface.

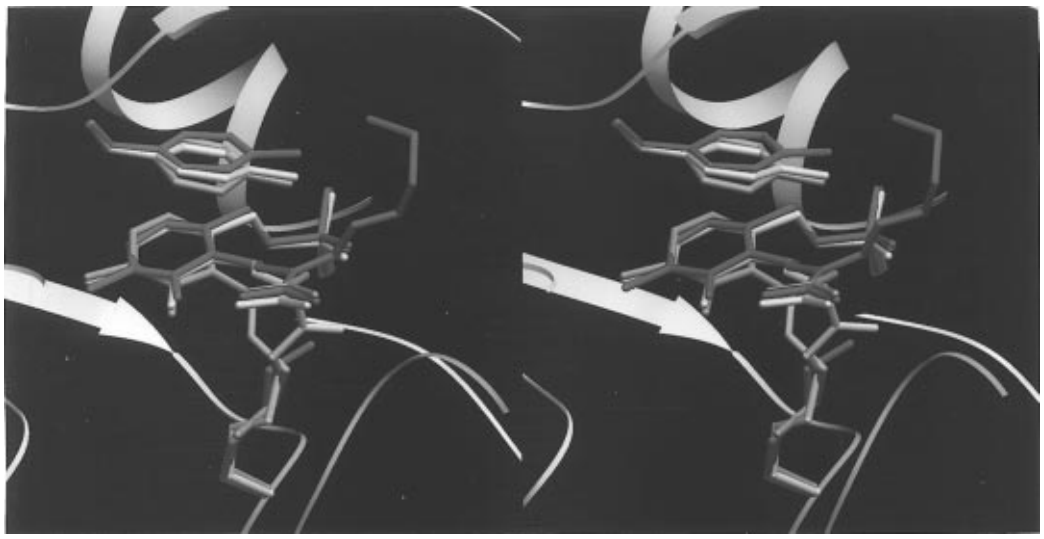

FIGURE 9: Stereoview of a superposition of Tyr111 and the PLP dervivative of the unliganded enzyme (magenta), the CBLAVG adduct (green), and the trifluoroalanine-inactivated enzyme (yellow).

static optimization, the whole model was fixed except for the terminal part of the inhibitor and its contacting protein groups. The final model structure is shown in Figure 8. The only difference from the CBLAVG complex is another hydrogen bond between the hydroxyl group of rhizobitoxine and Tyr238* which should lead to further stabilization of the EI* complex and a decreased dissociation constant K_i*. The results of Owens et al. (*8*) confirm this prediction; they reported for the *Salmonella typhimurium* CBL a K_i* value of 2.2×10^{-8} M.

In the recently solved crystal structure of the trifluoroalanine-inactivated CBL (*2*), the inactivator is bound similarly with respect to the cofactor to that seen in the complex with the slow-binding inhibitor AVG (Figure 9). The main difference is the location of Cβ and its substituents; in the trifluoroalanine complex, the inactivator is directed toward the protein interior [the A face of the cofactor (*47*)], whereas in CBLAVG, Cβ is located at the B side of the cofactor. Presumably, these two structures correspond to two possible steric conformations of the external aldimine, conformations that favor reactions either at Cβ or at Cγ. To achieve these conformations, it is necessary to postulate rotational freedom around the Cα−Cβ bond of the inhibitors in the external aldimine. Differences in the degree of rotation around Cα−Cβ allow partitioning between different chemical reaction types found in the γ-family of PLP-dependent enzymes, i.e. β-elimination, β-replacement, γ-elimination, and γ-replacement. Rotation around Cα−Cβ should mainly depend on the substituent at Cβ and on the chemical nature of the terminal substituent of the side chain. Remarkably, residues which are thought to interact with these groups and thereby determine the rotational freedom around Cα−Cβ are not conserved in the γ-family. Similar results demonstrating the catalytic importance of the electronegativity of the Cβ-substituent were obtained by Posner and Flavin (*48*). We propose that an ω-loop located in the C-terminal domain of CBL, containing residues Tyr338, Ser339, and Trp340, determines whether the β-substituent of the PLP−substrate aldimine is bound in a *trans* or in a *cis* orientation relative to the Hα atom (i.e. *cis* or *trans* to the Nα atom). According to the hypothesis of Braunstein (*49*), the former orientation should be found in β-eliminating lyases while the opposite one is proposed to occur in replacement-specific β-lyases.

However, the binding mode of AVG should be different from the productive substrate binding mode of CBL due to the lack of the terminal carboxylate group and the absence of the nucleophilic Sγ. Substrates of cystathionine γ-lyase and γ-synthase exhibit similar characteristics. Therefore, the CBLAVG Michaelis complex should rather approximate ES complexes of these enzymes. Further evidence stems from the short distance between the hydroxyl group of Tyr111 and Cγ, since Tyr111 has been proposed to be an acid−base catalyst in the active site of cystathionine γ-lyase and γ-synthase acting at the Cγ position of substrates and inhibitors (*2*, *50*).

Finally, the inhibitory activity of AVG and rhizobitoxine toward PLP-dependent enzymes involved in microbial and plant methionine biosynthesis and their low reactivity toward related mammalian enzymes suggest a potential use of these toxins as antibiotics and/or herbicides. Our X-ray structure of the CBLAVG complex should be helpful in the improvement of these inhibitors and may guide site-directed mutagenesis of specific active site residues which are thought to determine the substrate/inhibitor specificity and the type of reaction catalyzed by these enzymes.

ACKNOWLEDGMENT

We are grateful to the laboratory of Dr. S. Ghisla for providing access to the stopped-flow apparatus and to Margrit Jenny for recording excellent crystal spectra. We thank Dr. T. Mather for critical reading of the manuscript and Dr. J. N. Jansonius for helpful discussion.

REFERENCES

1. Dwivedi, C. M., Ragin, R. C., and Uren, J. R. (1982) *Biochemistry 21*, 3064−3069.
2. Clausen, T., Huber, R., Laber, B., Pohlenz, H.-D., and Messerschmidt, A. (1996) *J. Mol. Biol. 262*, 202−224.
3. Alexander, F. W., Sandmeier, E., Mehta, P. K., and Christen, P. (1994) *Eur. J. Biochem. 219*, 953−960.
4. Silverman, R. (1988) *Mechanism-based enzyme inactivation: chemistry and enzymology*, Vol. 2, CRC Press, Boca Raton, FL.
5. Silverman, R. B., and Abeles, R. H. (1976) *Biochemistry 15*, 4718−4723.
6. Pruess, D. L., Scannell, J. P., Kellet, M., Ax, H. A., Janecek, J., Williams, T. H., Stempel, A., and Berger, J. (1974) *J. Antibiot. 27*, 229−233.
7. Martel, A., Bouthier de la Tour, C., and Le Goffic, F. (1987a) in *Biochemistry of Vitamin B_6*, pp 341−344, Birkhäuser, Basel.
8. Owens, L. D., Guggenheim, S., and Hilton, J. L. (1968) *Biochim. Biophys. Acta 158*, 219−225.
9. Giovanelli, J., Owens, L. D., and Mudd, S. H. (1972) *Plant Physiol. 51*, 492−503.
10. Rando, R. R. (1975) *Acc. Chem. Res. 8*, 281−287.
11. Minamisawa, K., Fukai, K., and Asami, T. (1990) *J. Bacteriol. 172*, 4505−4509.
12. Morrison, J. F. (1982) *Trends Biochem. Sci. 7*, 102−105.
13. Laber, B., Clausen, T., Huber, R., Messerschmidt, A., Egner, U., Muller-Fahrnow, A., and Pohlenz, H.-D. (1996) *FEBS Lett. 379*, 94−96.
14. Uren, J. R. (1987) *Methods Enzymol. 143*, 102−105.
15. Cha, S. (1975) *Biochem. Pharmacol. 24*, 2177−2185.
16. Cha, S. (1976) *Biochem. Pharmacol. 25*, 2695−2702.
17. Morrison, J. F., and Walsh, C. T. (1988) *Adv. Enzymol. Relat. Areas Mol. Biol. 61*, 201−301.
18. Bradford, M. M. (1976) *Anal. Biochem. 72*, 248−254.
19. Raichle, T. (1981) *Untersuchungen zum Reaktionsmechanismus der Acyl-CoA Dehydrogenasen*, Ph.D. Thesis, University of Konstanz, Konstanz, Germany.
20. Leslie, A. G. W. (1990) in *Crystallographic Computing*, Oxford University Press, Oxford.
21. Collaborative Computational Project (1994) *Acta Crystallogr. D 50*, 760−763.
22. Brünger, A. T. (1992) *XPLOR (Version 3.1) Manual*, Yale University Press, New Haven, CT.
23. Jones, T. A., and Kjelgaard, M. (1991) *O—The Manual*, University of Uppsala, Uppsala, Sweden.
24. Scannell, J. P., Pruess, D. L., Demmy, T. C., Sello, L. H., Williams, T. H., Stempel, A., and Berger, J. (1972) *J. Antibiot. 27*, 229−233.
25. Rando, R. R., Relyea, N., and Chong, L. (1976) *J. Biol. Chem. 251*, 3306−3312.
26. Miles, w. (1975) *Biochem. Biophy. Res. Commun. 66*, 94−102.
27. Laber, B., Gerbling, K.-P., Harde, C., Neff, K.-H., Nordhoff, E., and Pohlenz, H.-D. (1994) *Biochemistry 33*, 3413−3423.
28. Laskowski, R. A., MacArthur, M. W., Moss, D. S., and Thornton, J. M. (1993) *J. Appl. Crystallogr. 26*, 283−291.
29. Ivanov, V. I., and Karpeisky, M. Y. (1969) *Adv. Enzymol. 32*, 21−53.
30. Rando, R. R. (1974) *Nature 250*, 586−587.
31. Gehring, H., Rando, R. R., and Christen, P. (1977) *Biochemistry 16*, 4832−4836.
32. Fersht, A. (1984) *Enzyme structure and mechanism*, Freeman, San Francisco.
33. Erion, M. D., and Walsh, C. T. (1987) *Biochemistry 26*, 3417−3425.
34. Badet, B., and Walsh, C. T. (1985) *Biochemistry 24*, 1333−1341.
35. Duncan, K., Faraci, W. S., Matteson, D. S., and Walsh, C. T. (1989) *Biochemistry 28*, 3541−3549.
36. Copie, V., Faraci, S., Walsh, C. T., and Griffin, R. G. (1988) *Biochemistry 27*, 4966−4970.
37. Dawson, R. M. C., Elliot, D. C., Elliot, W. H., and Jones, K. M. (1986) *Data for biochemical research*, 3rd ed., Clarendon Press, Oxford.
38. Hayashi, H., Inoue, Y., Kuramitsu, S., Morino, Y., and Kagamiyama, H. (1990) *Biochem. Biophys. Res. Commun. 167*, 407−412.
39. John, R. A. (1995) *Biochim. Biophys. Acta 1248*, 81−96.
40. Brzovic, P., Litzenberger Holbrook, E., Greene, R. C., and Dunn, M. F. (1990) *Biochemistry 29*, 442−451.
41. Sandmeier, E., and Christen, P. (1982) *J. Biol. Chem. 257*, 6745−6750.
42. Kirsch, J. F., Eichele, G., Ford, G. C., Vincent, M. G., Jansonius, J. N., Gehring, H., and Christen, P. (1984) *J. Mol. Biol. 174*, 497−525.
43. Cronin, C. N., and Kirsch, J. F. (1988) *Biochemistry 27*, 4572−4579.
44. Johnston, M., Raines, R., Chang, M., Esaki, N., Soda, K., and Walsh, C. T. (1981) *Biochemistry 20*, 4325−4333.
45. Karube, Y., and Matsushima, Y. (1977) *J. Am. Chem. Soc. 99*, 7356−7358.
46. Engh, R. A., and Huber, R. (1991) *Acta Crystallogr. A 47*, 392−400.
47. Ford, G. C., Eichele, G., and Jansonius, J. N. (1980) *Proc. Natl. Acad. Sci. U.S.A. 77*, 2559−2563.
48. Posner, B. I., and Flavin, M. (1972) *J. Biol. Chem. 247*, 6412−6419.
49. Braunstein, A. E., and Goryachenkova, E. V. (1976) *Biochimie 58*, 5−17.
50. Washtien, W., and Abeles, R. H. (1977) *Biochemistry 16*, 2485−2491.

BI970630M